

Improving solvent-based self-healing materials through shape memory alloys

S. Neuser^{a,*}, V. Michaud^a, S.R. White^b

^a *Laboratoire de Technologie des Composites et Polymères (LTC), Institut des Matériaux, Ecole Polytechnique Fédérale de Lausanne (EPFL), CH-1015 Lausanne, Switzerland*

^b *Departments of Aerospace Engineering, Beckman Institute for Advanced Science and Technology, University of Illinois at Urbana-Champaign, Urbana, IL 61801, USA*

ARTICLE INFO

Article history:

Received 10 October 2011

Received in revised form

5 December 2011

Accepted 6 December 2011

Available online 19 December 2011

Keywords:

Self-healing polymer

Smart composite

Solvent

ABSTRACT

Healing of epoxy resins can be accomplished using a combination of embedded ethyl phenylacetate (EPA) solvent loaded capsules and shape memory alloy (SMA) wires. Upon crack formation, the EPA solvent diffuses in the resin and induces swelling which tends to close the crack, while the SMA wires upon heating reduce the crack gap and foster residual epoxy cure. The kinetics of EPA diffusion in the epoxy matrix were measured so as to evaluate the swelling thickness versus time, and concentration at saturation. The largest healable crack gap was found to be 30 μm after 24 h. EPA solvent was shown to lower the curing reaction kinetics and the glass transition temperature (T_g) of the epoxy, as well as its stiffness and strength. Healing efficiency was assessed using long-groove tapered double cantilever beam (TDCB) test samples, with embedded SMA wires across the crack plane. The healing efficiency greatly improved when the crack gap was reduced to 30 μm , from 24% for samples without SMA wires to 78% for samples with SMA wires activated according to an optimized scenario.

© 2011 Elsevier Ltd. All rights reserved.

1. Introduction

Self-healing materials exhibit the ability to repair themselves and to recover functionality using the resources inherently available to them [1–3]. Two primary classes of self-healing have emerged: intrinsic and extrinsic systems [4]. Intrinsic systems recover from damage through an inherent property of the material (e.g. increasing molecular mobility by heating a thermoplastic above its glass transition temperature (T_g) or exploiting reversible crosslinking reactions). Extrinsic systems rely on incorporating secondary materials (healing agents), usually a liquid phase, that is released upon damage and fills the damage volume. A similar classification scheme was introduced by Bergman et al., who distinguished between reversible and irreversible systems [5]. In almost all cases, intrinsic systems can repeatedly heal damage, so that healing can occur more than once at the same location because the mechanism is based on a reversible chemical or physical process. On the other hand, extrinsic systems are irreversible as the healing agent is depleted after a healing event. An exception to this rule is microvascular delivery systems, where the healing agent is continuously provided through a network of microchannels [6–13]. While intrinsic systems only heal when the crack faces are in close contact as the molecules cannot bridge large crack gaps,

extrinsic systems demonstrated healing for larger crack gaps, depending on the accessible volume of healing agent within the damage zone [14]. Furthermore, intrinsic systems mostly rely on heating to induce healing. Depending on the chemical systems, these temperatures are often in excess of 100 °C. As an example, reactions of the Diels–Alder (DA) type have a threshold temperature at which the two components dissociate at about 150 °C [2]. When cooling down, the bonds are reformed through the reverse Diels–Alder (rDA) reaction. The heat–cool cycle also leads to a loss of mechanical properties of the affected area during heating.

The extent of the damage to repair is critical in selecting an appropriate repair strategy. Small damage in coatings or micro-cracks could be healed with intrinsic systems while macroscopic damage with substantial crack volume needs an extrinsic system. Whichever approach is used, reducing the damage volume is beneficial to improving healing performance and reducing the required volume of healing agent. Kirkby et al. [15] investigated the effect of reducing crack separation by activating embedded shape memory alloy (SMA) wires to close the crack in epoxy fracture samples using a DCPD/Grubbs' healing system. Healing efficiency as measured through the recovery of fracture toughness was increased by a factor of 1.6 for manually injected samples through a combination of reduced crack gap and localized heating of the crack plane as a result of SMA wire activation. Fully in-situ healing was then demonstrated for self-healing epoxy with embedded DCPD micro-capsules and Grubbs' catalyst particles [14]. The healing efficiency showed a strong dependency on the crack gap. For the smallest

* Corresponding author. Tel.: +41 216 934 836.
E-mail address: sam.neuser@epfl.ch (S. Neuser).

gaps, healed peak loads of 60 N were measured, representing 80% of the virgin properties. In stark contrast, for samples without SMA wires, the average healed peak load was only about 18 N.

Among the various healing systems investigated so far, some of these healing systems used diffusion based healing mechanisms. Hayes et al. [16] mixed up to 20% of a thermoplastic to an epoxy matrix which acted as a healing agent when heated. Mookhoek et al. [17] analyzed healing in a thermoplastic material, containing microencapsulated solvent as a healing agent. Caruso et al. [18] recently proposed a solvent-based healing system for thermosetting polymers (e.g. epoxy). Upon damage, the solvent is released onto the fracture surface, increasing local chain mobility and promoting the reaction of residual hardener with either residual epoxide groups in the matrix, or a small volume of epoxy resin delivered with the solvent [19]. While it was first demonstrated for chlorobenzene, a less toxic solvent (ethyl phenylacetate, or EPA) mixed with a few percent of epoxy was shown to yield nearly 100% healing efficiency and long term stability was preserved even after 30 days. However, this excellent healing efficiency was only achieved in a modified TDCB sample geometry that maintained crack faces in close contact after fracture, thus minimizing the damage volume to heal, known as short-groove TDCBs.

In this article, we evaluated the healing of epoxy using solvent microcapsules combined with embedded SMA wires. The combination of the two concepts should allow the healing of larger damage volumes as is encountered in standard TDCB geometries. To optimize the healing process, we investigated the mechanisms of solvent healing by analyzing the diffusion kinetics of the solvent in the epoxy matrix. We experimentally determined swelling of the thermoset resin due to the solvent diffusion and quantified the effect of the solvent on the matrix in terms of residual heat of reaction as well as mechanical properties. We finally investigated the effect of SMA wire activation on the healing efficiency of TDCB samples, for various configurations.

2. Materials and methods

2.1. Materials

The epoxy resin used was Epon 828, a DGEBA epoxy resin (Shell Chemicals). It was mixed with diethylenetriamine (DETA, Sigma–Aldrich) as a curing agent in a 100:12 ratio. Curing took 24 h at ambient temperature followed by 24 h at 35 °C. Ethyl phenylacetate (EPA 99%, Sigma–Aldrich) was used as the healing agent. The SMA wire used in this study was a martensitic NiTiCu alloy with respective composition of 44.86/45.08/10.06 and a diameter of 150 μm (Furukawa Techno Material). The phase transition temperatures were determined using differential scanning calorimetry (DSC). Any previous deformation history was erased by performing a first heat–cool cycle between 10 and 100 °C and the phase transition temperatures were then determined during a second heat–cool cycle between 10 and 120 °C. They are summarized in Table 1.

2.2. Encapsulation and stability

The microcapsules were produced using the protocol developed by Blaiszik et al. [20]. In the present work, the core liquid

was composed of 97.5% EPA and 2.5% Epon 828 as this ratio was shown to provide the best healing efficiency through formation of additional thermoset material in the crack plane [19]. The emulsion was stirred at a rate of 400 rpm and after the urea-formaldehyde (UF) reacted to form the shell wall the microcapsules were dried in ambient air for at least 24 h, then mechanically sieved, retaining the fraction between 125 and 355 μm . The mean diameter was measured using optical microscopy, taking an average of at least 100 measurements. For comparison purposes, a batch of DCPD containing microcapsules was prepared using the protocol defined by Brown et al. and a stirring rate of 550 rpm [21]. Stability of microcapsules was evaluated by thermal gravimetric analysis (TGA) on a Mettler Toledo sDTA851e. The capsules were kept at ambient conditions for several days before running the TGA measurements, so moisture intake was possible. Capsules were loaded in the TGA and were heated from 30 to 400 °C at 10 °C/min in a N_2 atmosphere. The results were then related to the capsule stability by comparing the boiling temperatures of the core material to the capsule weight loss profile.

2.3. Solvent diffusion

The first set of experiments to quantify the swelling of epoxy in pure EPA solvent were carried out using cylindrical epoxy samples of 9.7 mm diameter and a height of 4.9 mm (ca. 0.42 g), which were immersed into the solvent. Weight uptake was measured using a high-resolution precision balance (Mettler Toledo AT261 DeltaRange, 0.01 mg reading, repeatability 0.015 mg). To do so, the samples were taken out of the solvent and dried on the surface using Kimtech Precision Wipes (Kimberly Clark, ref. 7552) before weighing. The error due to residual solvent on the sample surface was estimated to be less than 0.04% for this test configuration.

After 3 weeks of immersion in the solvent, the samples were cleaved along the axis of the cylinder and the crack faces were observed under a Olympus stereo-microscope. Presence of solvent in the diffusion layer was measured with an FTIR microscope (PerkinElmer Spotlight FTIR Imaging).

Since the diffusion kinetics of EPA in epoxy are relatively slow, a second set of experiments using smaller samples (from ca. 0.2 to 6 mg) were prepared in order to determine the solvent solubility at saturation. After 3 weeks immersion, these samples were dried on the surface, weighed, and weight uptake was calculated.

2.4. TDCB sample preparation

The long-groove TDCB sample preparation with integrated SMA wires followed the procedure described by Kirkby et al. [15] with minor modifications. The long-groove TDCB geometry is shown in Fig. 1. The samples were prepared in two steps: first the surrounding matrix including the SMA wires were cast into silicone molds using pure epoxy resin. After 4 h, the inner part of the sample was cast using epoxy resin mixed with 15 wt% of microcapsules containing the healing agent (97.5% EPA and 2.5% Epon 828). In parallel, to provide a benchmark for healing results, short-groove samples without SMA wires were also prepared. Short-groove samples are geometrically identical to the long-groove TDCBs, however the central groove only extends 25 mm from the notch allowing the crack to arrest after fracture so that the crack faces maintain registration and the crack gap is minimized [19].

Previously, Kirkby et al. [15] included clamps on the SMA wires at the surface of the TDCB specimen in order to ensure good load transfer of recovery force from the wires to the specimen. In this

Table 1
Phase transition temperatures for the SMA wire.

	A_s	A_f	M_s	M_f
T [°C]	54.3	60.6	44.3	37.3

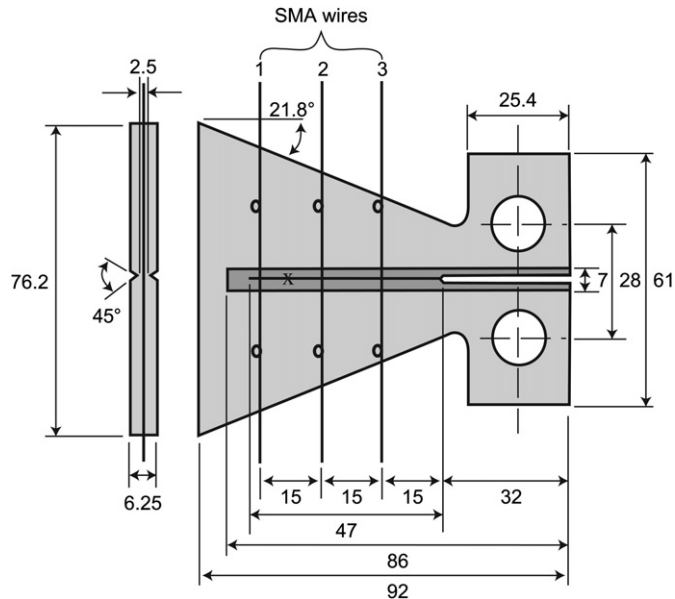


Fig. 1. Schematic of the TDCB geometry with 3 SMA wires, anchored with knots. The SMA wires are evenly spaced, perpendicular to the crack axis. The knots in each wire are 3 cm apart, 1.5 cm from the center of the sample. The location of the thermocouple used to measure the temperature inside of the sample is marked with an x, between the left and middle SMA wire. Dimensions in mm.

work we introduce a simpler method of force transmission under the form of overhand knots, anchored in the matrix (see Fig. 1). The knots are separated by about 3 cm, allowing an absolute crack separation of 1.8 mm (6% wire strain) before irreversible plastic deformation occurs in the SMA wire. This is largely sufficient in comparison to the maximum achieved displacement of about 1 mm during a TDCB test. Anchoring knots could be introduced in fiber reinforced composites relatively easily through weaving or stitching processes.

Using the formula developed by Rule et al., we can calculate the healing agent delivered per unit crack area, D_h using Eq. (1) [22].

$$D_h = \rho_m \phi d_c \quad (1)$$

where ρ_m is the matrix density, ϕ is the weight fraction of microcapsules and d_c is the average volume weighted diameter of the capsules. In our case this yields 4.97 mg/cm², enough healing agent to fill a crack gap of about 48 μ m.

2.5. Healing test

Healing performance was assessed through fracture testing of TDCB samples loaded in tension at a displacement rate of 5 μ m/s. Virgin samples were precracked by tapping a razor blade into the molded starter-notch, fractured, then left to heal according to a given scenario with or without heating of the SMA wires, and tested again. The crack gap was optically measured immediately after SMA wire activation. In general, the crack gap was not distinguishable anymore after the healing period of 24 h. The crack disappearance is a necessary but not sufficient condition for successful crack healing.

When wire heating was used, a constant electrical current of 0.5 A per wire was applied. The corresponding temperature profile inside the TDCB sample was measured with small diameter integrated thermocouples (= 0.5 mm) attached to the embedded SMA wire and at a location in the central groove, between two SMA

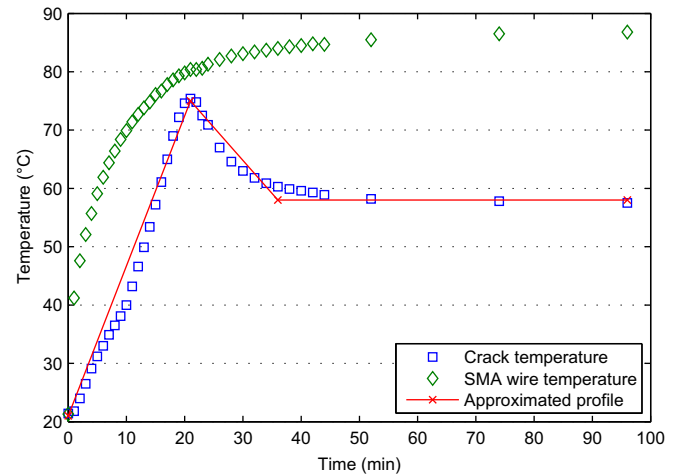


Fig. 2. Measured temperature profile for a TDCB sample during SMA wire activation. The drop in crack temperature after a peak temperature of about 75 °C is due to SMA wire debonding.

wires (as indicated in Fig. 1). The measured temperature profiles are given in Fig. 2. The wires reach about 90 °C after 1 h while the epoxy matrix in the central groove stabilizes at 60 °C after a peak at 75 °C. This drop of temperature after reaching the peak value is due to the debonding of the wire, leading to reduced thermal conductivity through the interface.

The healing efficiency η is defined as the ratio of the healed and virgin fracture toughnesses, which for the TDCB geometry reduces to the healed peak load P_h over the virgin peak load P_v [23].

2.6. Thermal and curing behavior

To quantify the effect of the diffused solvent on the T_g and latent reactivity of the resin, DSC (TA Q100) tests were carried out using a modulated temperature ramp of 2 °C/min from 20 °C to 160 °C on samples of weight 5–10 mg. The modulation amplitude was ± 1 °C and the modulation period was 40 s. These settings were necessary as the T_g was superposed with the enthalpic relaxation. We analyzed the curing process of Epon 828 with DETA in presence of EPA solvent by oscillatory shear

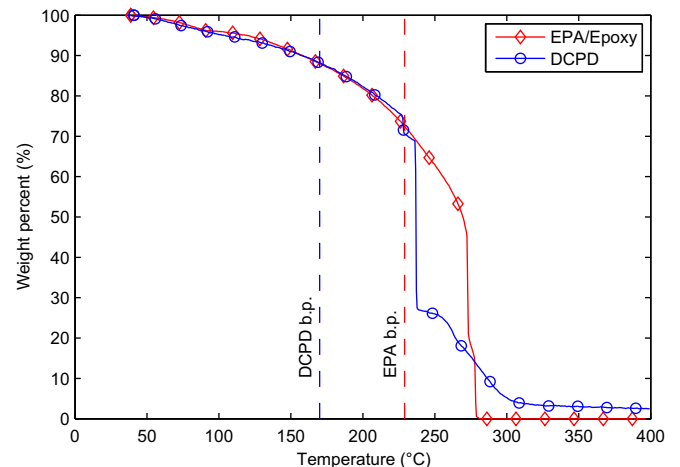


Fig. 3. TGA results for DCPD and EPA microcapsules. Vertical lines denote DCPD and EPA boiling points. The heating rate was 10 °/min.

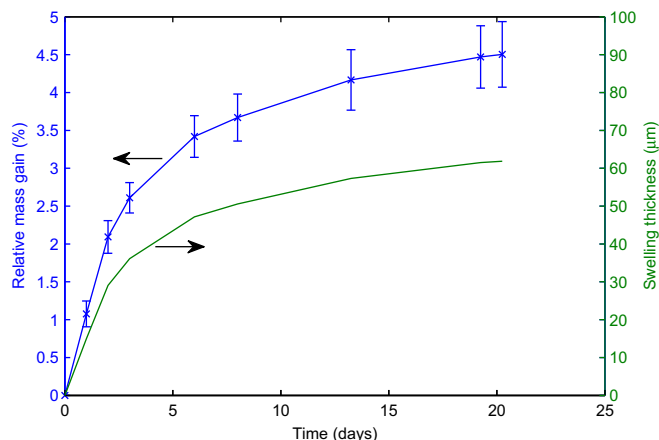


Fig. 4. Evolution of the average weight of epoxy cylinders immersed in EPA solvent over 3 weeks as well as the corresponding swelling.

rheology between parallel plates of 25 mm diameter (TA AR200ex). The tests were performed at 1 Hz and 0.1% strain, at room temperature or using a temperature profile similar to the conditions found during activation of the SMA wire (see Fig. 2). The temperature profile was approximated by a heating ramp to 75 °C in 21 min, followed by a cooling ramp to 58 °C in 15 min and a plateau temperature of 58 °C for the remaining time of the test. The gel point was taken at the crossover of the shear storage modulus G' and shear loss modulus G'' [24].

Furthermore, we measured the mechanical properties of the resin prepared without solvent and with EPA solvent at the saturation concentration, c_{sat} . This test was carried out using a dogbone geometry (ASTM D638) and the Young's modulus, elongation at break and ultimate strength were measured on a UTS tensile testing machine at a displacement rate of 50 $\mu\text{m/s}$.

3. Results

3.1. Microcapsule characterization

The volume weighted average diameter for the EPA/epoxy microcapsules was found to be $d_V = 286 \mu\text{m}$ (number weighted average diameter $d_n = 230 \mu\text{m}$). The DCPD microcapsules had a volume weighted average diameter of $d_V = 238 \mu\text{m}$ (number weighted average diameter $d_n = 202 \mu\text{m}$). TGA measurements showed that the capsules protect the healing agent up to the boiling temperature of their content. Fig. 3 compares results of DCPD and EPA/epoxy capsules, stored at room temperature. Around 100 °C, a 5% weight loss took place due to water evaporation as the microcapsules were not dried before the test. Both microcapsule types presented a 50% weight loss only well beyond the respective boiling temperature of the liquid cores.

3.2. Diffusion and swelling

The results of solvent diffusion tests are shown in Fig. 4. Relative mass gain increased to 4.5% after 3 weeks (average over 3 samples). Fig. 5 shows an optical image of the cleaved cylinder sample after 3 weeks revealing the presence of a skin region that exhibits ductile fracture (thickness of the ductile layer is shown for different locations) while the interior of the sample shows brittle fracture. Furthermore, the skin region was soft, almost gel-like, as opposed to the unaffected brittle core with a sharp interface. The average thickness of this ductile layer was $213 \pm 44 \mu\text{m}$ after 3 weeks.

Such a sharp diffusion front has been observed previously for solvent diffusion through polymers [25,26] and is commonly referred to as Case II diffusion. In this case, the solvent concentration is constant on the surface up to the diffusion front of length l_D and drops rapidly toward zero beyond the diffusion front. In order to confirm a Case II diffusion, a line scan was performed using an FTIR microscope. To increase the signal to noise ratio, the aperture

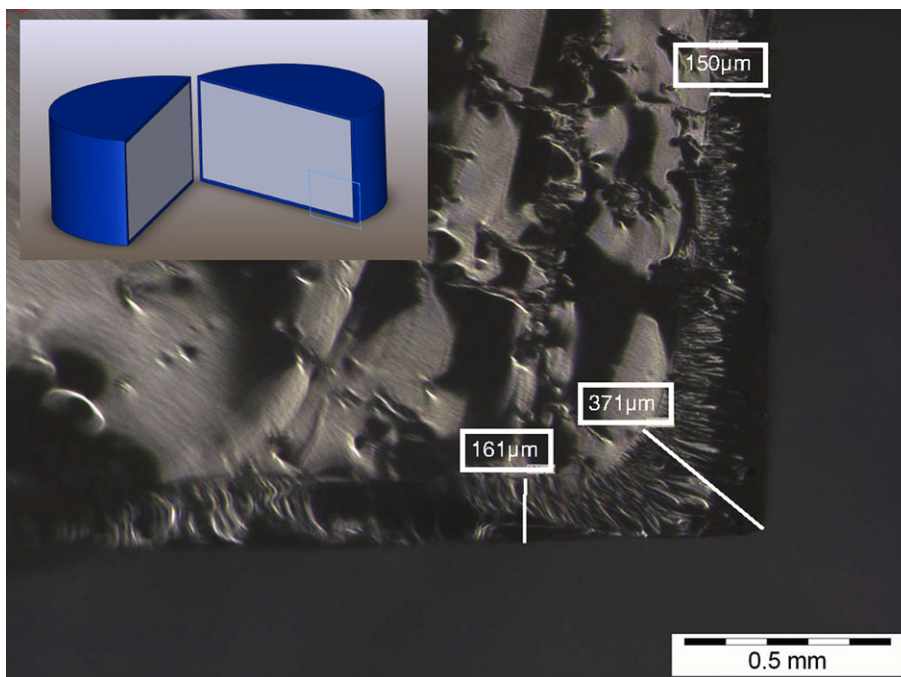


Fig. 5. Image showing a corner of the cylinder's fracture face after the swelling experiment (as indicated in the schematic inset). We can distinguish the mirror like, unaffected core of the cylinder and the gel-like surface layer.

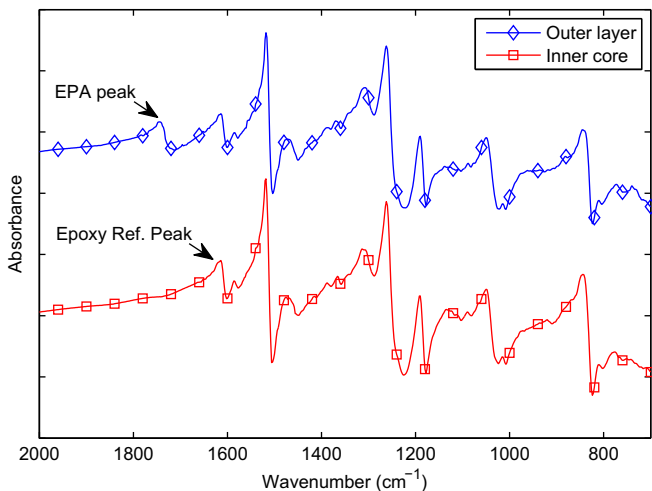


Fig. 6. Comparison of IR spectra of unaffected core and surface layer. Absorbance peaks are detected at 1616 and 1743 cm^{-1} associated with the phenoxy group of the Epon 828 and the phenyl substituted carboxylic acid ester of EPA, respectively.

size was 50 μm and the spectra were averaged over 16 acquisitions. In Fig. 6, we compare the spectra measured at the unaffected core (position 50 μm in Fig. 7) and the surface layer (position 250 μm in Fig. 7). Data was collected from 4000 to 700 cm^{-1} and a baseline correction was applied. For clarity, only the range where relevant peaks were observed, from 2000 to 700 cm^{-1} , is shown. Specifically we observed absorbance peaks at 1616 and 1743 cm^{-1} associated with the phenoxy group of the Epon 828 and the phenyl substituted carboxylic acid ester of EPA, respectively. These peaks were also confirmed in separate IR spectra of pure epoxy and EPA respectively.

In Fig. 7, we plotted the single wavenumber profile of the 1743 cm^{-1} peak vs. the 1616 cm^{-1} peak. The sudden increase of EPA signal at 200 μm roughly coincides with the observed diffusion length.

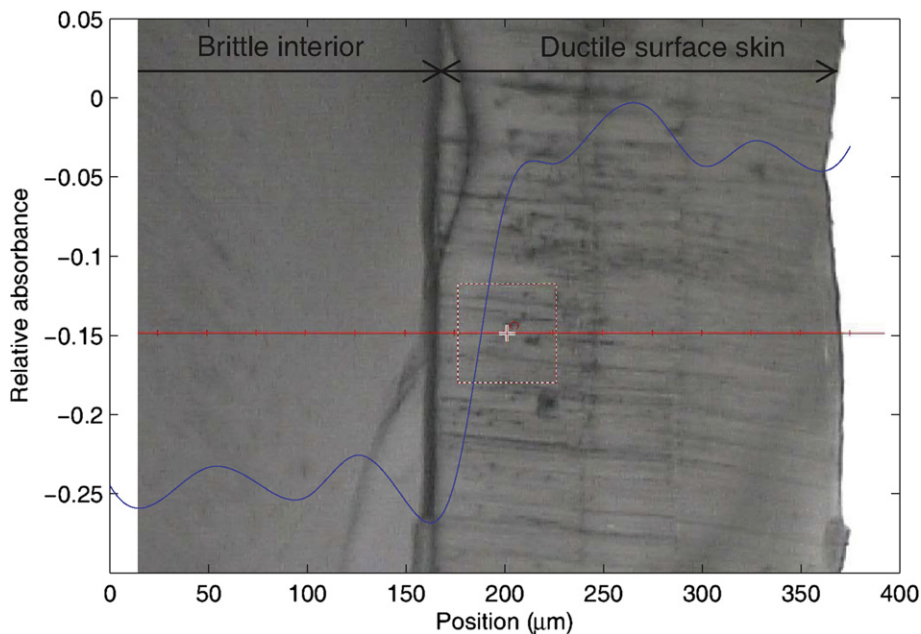


Fig. 7. FTIR line scan along cleaved sample surface. Relative absorbance of the peak heights (1743 vs. 1616 cm^{-1}) plotted as a function of position showing a clear demarcation corresponding to the solvent swollen skin region.

3.3. Geometric swelling

In order for solvent-induced healing to occur the affected crack faces must be in intimate contact. As such, the amount of swelling that occurs through solvent diffusion is an important parameter dictating the maximum amount of crack separation before healing can no longer occur. We modeled the geometric swelling of epoxy by assuming a square solvent concentration profile: a constant concentration until the diffusion front and zero concentration at the diffusion front and beyond. More complex models do exist but are beyond the scope of this work [27,28], since we are primarily interested in evaluating the thickness of the solvated layer.

Assuming that all weight increase occurs through solvent uptake then the change in volume (ΔV) is related to the mass increase m_i through the solvent density ρ_s of EPA (1030 kg/m^3) [28]. Substituting for the initial and final volume yields a 3rd order polynomial for the swelling thickness t_s (Eq. (2)),

$$\Delta V = V_f - V_i = \frac{m_i}{\rho_s} = 2\pi r t_s^3 + (4\pi r + \pi h) t_s^2 + (2\pi r^2 + 2\pi r h) t_s \quad (2)$$

where r and h are the radius and height of the cylinder respectively. Note that we neglect the influence of curvature on the value of t_s as well as edge effects as the radius $r \gg t_s$.

The swelling thickness as a function of time is plotted in Fig. 4. After 24 h, the solvent film thickness t_s of about 15 μm and after 3 weeks the swelling thickness is 62 μm . Dividing t_s by the thickness of the saturated, gel-like layer (213 μm) gives us a rough estimate of the optically measured saturation concentration c_{opt} of EPA in the gel and c_{opt} is found to be around 29%.

3.4. Saturation concentration

To confirm these first results of the EPA saturation concentration in the epoxy matrix, we immersed very small samples (a few mg) in the solvent for 3 weeks. With the diffusion length of 213 μm , the maximum sample dimension should not exceed 426 μm . For a spherical sample shape, this translates into a maximum weight of

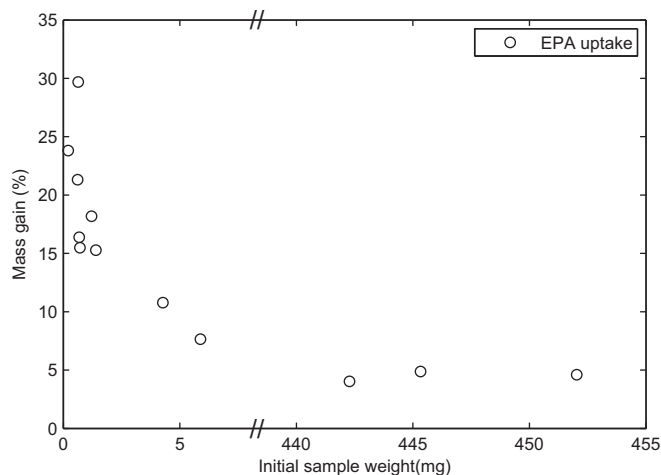


Fig. 8. Solvent uptake as a function of sample weight, immersed in EPA for 3 weeks.

about 0.047 mg. In practice, it is not feasible to produce such small samples, but for a thin rectangular shape, the maximum allowed weight is higher because the surface to volume ratio is higher. The sample weight varied from 0.21 to 5.88 mg. Results are displayed in Fig. 8, including the results of the first test series. As expected, the highest absorption results were achieved by the smallest samples at almost 30% weight increase (solvent concentration of 23% in the final weight).

For simplicity, we use the value of 25% of solvent concentration at saturation as a compromise between the optically determined saturation concentration (29%) and the saturation concentration calculated through the samples' weight increase (23%) for the following experiments.

3.5. DSC

In Figs. 9 and 10, we compare DSC thermograms of Epon 828/DETA samples immediately after curing and after 3 weeks immersion in pure EPA solvent. The enthalpic relaxation peak provides a very good estimate of the actual location of the T_g as shown by the step transition in the reversible heat flow in Fig. 9. In the plain epoxy, an enthalpic relaxation is observed at 68.6 °C. Heating above T_g immediately enables the latent functionalities to react, giving rise to an important exothermic peak in the non-reversing heat flow signal. The latent heat of reaction is found to be 148.50 J/g. For

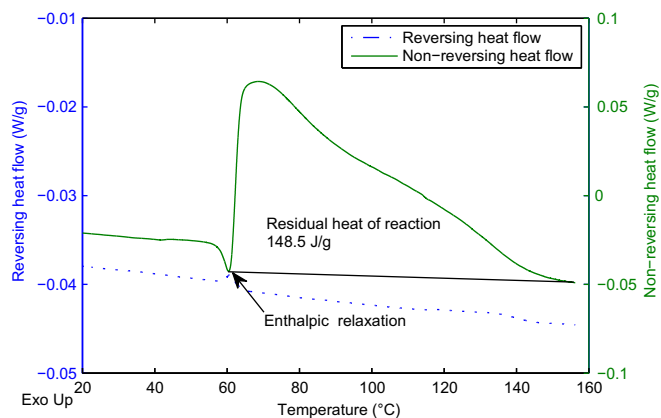


Fig. 9. Modulated DSC results for Epon 828/DETA cured for 24 h at room temperature and 24 h at 35 °C.

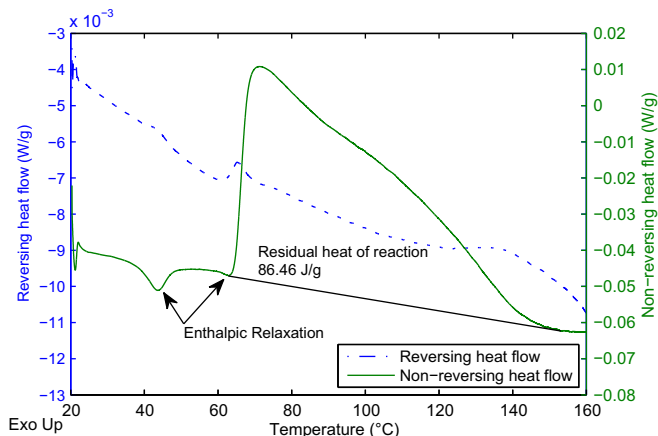


Fig. 10. Modulated DSC results for Epon 828/DETA cured for 24 h at room temperature and 24 h at 35 °C then immersed in EPA solvent for 3 weeks.

the sample immersed in solvent, these same processes are observed at very similar temperatures. The enthalpic peak is found at 71.3 °C, followed by the exothermic peak due to the latent functionality with a reduced latent heat of reaction of 86.46 J/g. A second enthalpic relaxation peak was also detected at 43.7 °C. To confirm that solvent in the diffused layer was responsible for the presence of a secondary peak, we also analyzed samples where the 25 wt% EPA solvent was directly mixed with the epoxy and DETA before casting and curing. The DSC thermogram in Fig. 11 shows no exothermic peak, indicating that all the monomer had reacted during the primary cure and a small enthalpic relaxation peak at 38.5 °C, corresponding to the T_g of the solvated epoxy.

The DSC results let us conclude that EPA solvent has major effects on the EPON 828/DETA matrix, namely a decrease of the matrix's T_g by about 30 °C and the reaction of residual functionalities. The DSC results for the sample immersed in EPA solvent showed a bimodal response which is due to the presence of the solvated surface layer and the unaffected interior of the sample.

3.6. Curing and mechanical properties

The curing of epoxy in presence of the solvent was measured by oscillatory rheometry. The presence of solvent largely delayed the gel point: 25% EPA solvent mixed with 67% resin and 8% hardener (standard 100:12 ratio between epoxy and hardener) delayed the gel time at room temperature from 3.5 h to 10 h. With heating

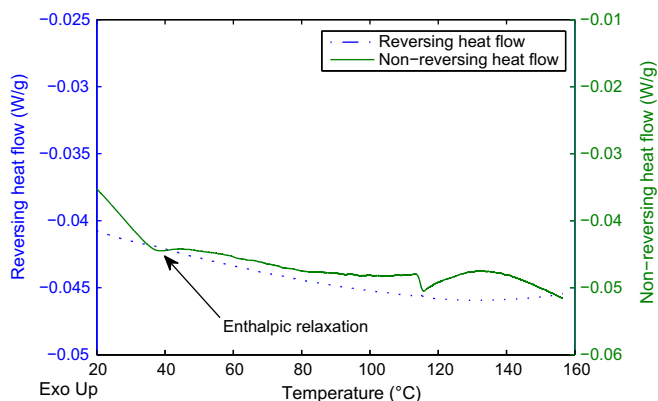


Fig. 11. Modulated DSC results for Epon 828/DETA with 25 wt% EPA cured for 24 h at room temperature and 24 h at 35 °C.

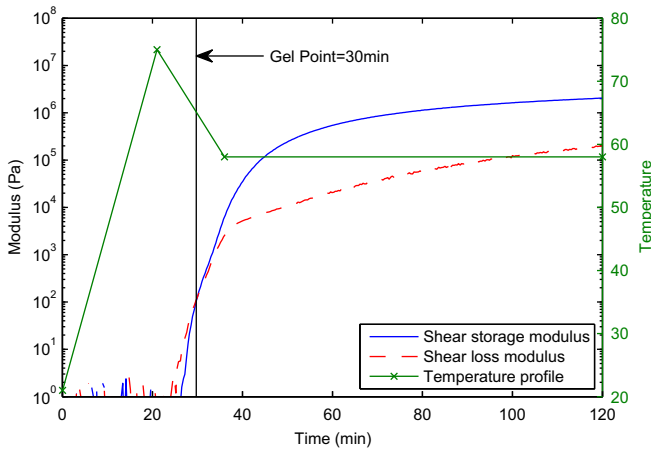


Fig. 12. Oscillatory rheometry test results for curing of Epon 828/DETA with 25 wt% EPA solvent.

through SMA wires, the gel point of the same resin/solvent mixture decreased to about 30 min, using a simulated temperature profile determined from the wire heating experiments (Fig. 12). The delay in curing in the presence of EPA solvent is due to the lower concentration of the reactive species caused by the “dilution” effect of the solvent. The concentration of solvent used was based on the saturation concentration of solvent in the matrix. In a real crack, the concentration of EPA solvent in the matrix surrounding the crack gap does not remain constant as the amount of solvent supply is limited. Once all the solvent solvated the matrix, diffusion sets in and the concentration will drop. The results described here should be considered as an approximation of the conditions in the crack.

Results of mechanical testing of samples cured with and without 25 wt% EPA solvent are presented in Table 2. EPA lowers both the Young’s modulus as well as the ultimate strength by a factor of more than 2 while the elongation at break is substantially increased.

3.7. Healing assessment

First, short-groove samples were prepared to validate the healing ability of the EPA/epoxy microcapsules prepared in this work. For samples containing 5% of EPA/epoxy microcapsules, we observed multiple healing events, with healing efficiencies reported in Table 3. The results compared well to the results by Caruso et al. [19].

Long-groove tapered double cantilever beam (TDCB) samples were then tested to measure virgin and healed fracture toughness.

Table 2
Mechanical properties of the resin cured with 25% solvent.

	Resin + EPA	Resin
Young’s modulus [GPa]	1.0 ± 0.0	2.54 ± 0.1
Ultimate strength [MPa]	20.9 ± 0.7	43.51 ± 5.7
Elongation at break [%]	5.7 ± 0.5	2.02 ± 0.3

Table 3
Healing of short-groove TDCBs, 5 wt% EPA/epoxy microcapsules, without SMA.

Heal event	Healing efficiency [%]
First healing	92.5 ± 10.5
Second healing	81.9 ± 12.2
Third healing	74.9 ± 7.6

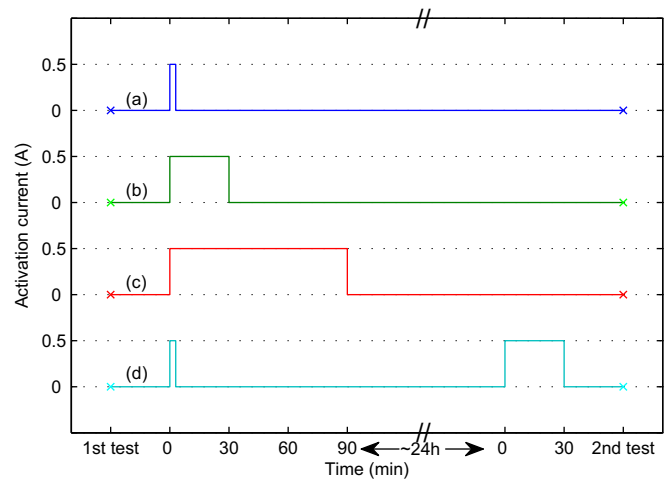


Fig. 13. Activation schedules for the different SMA activation profiles.

For the DCPD/Grubbs’ healing system, it was shown in earlier work that 30 min of wire activation was sufficient to achieve optimal healing [15]. However, in the present work, we investigated four different healing protocols in which the activation time was systematically increased along with a hybrid case where two separate activation events occurred over a 24 h healing period. Each healing protocol is depicted in Fig. 13 as a function of time after the virgin fracture event (1st test). In all cases, activation of the SMA wires is achieved by applying a constant 0.5 A current through the wire. Healed fracture testing was conducted 24 h after wire activation in all cases (2nd test).

Schedule (a) was chosen as it represents the minimum time to achieve a substantial crack closure without excessive heating of the sample (<30 °C after 3 min, see Fig. 2). Schedule (b) follows the optimal activation profile from Kirkby et al. [15] and is sufficient time to ensure gelation in the crack plane (see Fig. 12). Schedule (c) increases the activation time to 90 min to promote full crack closure and a higher degree of cure in the crack plane during activation. Schedule (d) was also investigated as an attempt to minimize initial activation time (similar to schedule (a)) while promoting a higher degree of cure of the healed material in the crack plane (similar to schedule (b)).

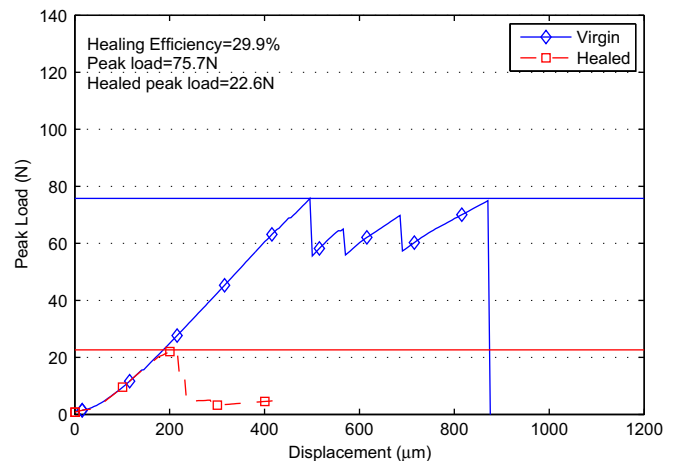


Fig. 14. Typical results for a TDCB healing test (sample without SMA wires, manually aligned). Virgin and healed force-displacement curves are shown and horizontal lines show the maximum achieved load.

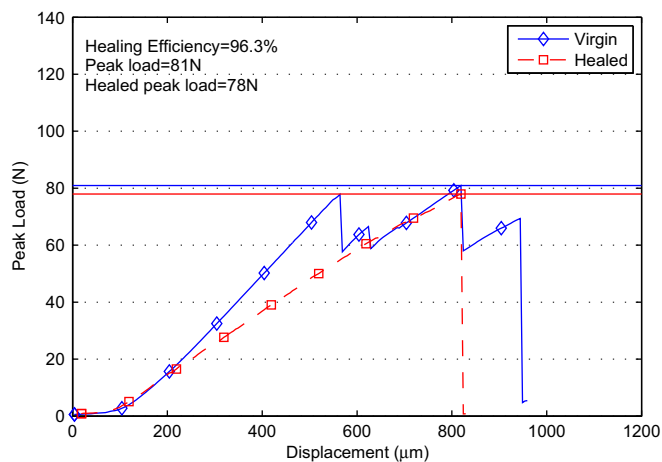


Fig. 15. Typical results for a TDCB healing test (sample activated for 90 min). Virgin and healed force-displacement curves are shown and horizontal lines show the maximum achieved load.

Examples of TDCB testing curves obtained on virgin and healed samples are given in Fig. 14 (control, no SMA) and Fig. 15 (activation schedule (c)). The manually clamped control sample showed poor healing efficiency with crack progradation already at around 23 N. In the sample with SMA wires, activated for 90 min after initial testing, we observe a first crack event already at around 20 N in the healed response. This behavior was frequently observed and might result from less efficient healing close to the starting notch, which is furthest from the SMA wires. The maximal load for the healed sample was only 3 N below that of the virgin sample in this particular case.

The results for the different activation schedules are presented in Table 4, listing the average healing efficiency of at least 6 samples, standard deviation, and average crack gap after SMA wire activation. The complete data set is represented graphically in Fig. 16 as a function of crack gap. There is a very strong correlation between healing efficiency and the size of the crack gap after wire activation. Above a critical crack gap of approximately 40 μm , samples failed to heal to any appreciable level. As the crack gap is reduced the healing efficiency is dramatically increased regardless of the specific activation schedule used.

In detail, the healing efficiency was increased stepwise from 26% to 35% to 71% to 78% when using 3 min, 3 min followed by 30 min the next day, 30 min and 90 min of SMA activation time after testing the samples, respectively. The crack gap after activation follows the same trend as former observations [15] even though the absolute values are higher in this work. While some samples activated for 30 min had similar crack gap values to the ones activated for 90 min, the lowest measured healing efficiency increased from 18% for 30 min to 57% for 90 min. This could indicate that when manipulating the samples after 30 min, they are still easily broken.

The maximum healable crack gap of 48 μm calculated using Eq. (1) is valid for 2-component healing agent chemistries such as the DCPD/Grubbs' system which fills the crack gap and forms a new

Table 4
Healing assessment results.

SMA schedule	Crack gap [μm]	Healing efficiency [%]
Control (no SMA)	27.3 \pm 9.4	24.3 \pm 16.2
(a)	43.4 \pm 32.1	25.9 \pm 25.1
(b)	16.8 \pm 14.0	70.5 \pm 28.3
(c)	11.9 \pm 5.9	78.2 \pm 20.6
(d)	32.5 \pm 8.8	34.8 \pm 47.8

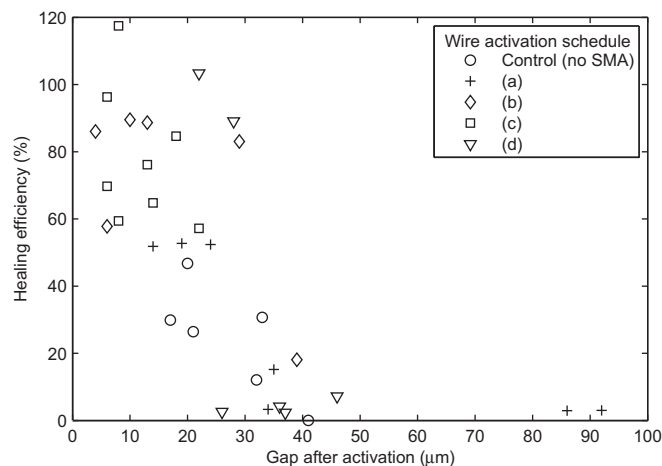


Fig. 16. Healing efficiency vs. measured crack gap after wire activation.

phase. However, for the solvent-based system where the solvent diffuses and swells the matrix it is clear that lower crack gaps are necessary and the crack separation should be substantially lower than the predicted 48 μm . From Fig. 4, the maximal crack gap beyond which the crack faces do not enter in contact is $2 \cdot 15 = 30 \mu\text{m}$ (after 24 h). This of course neglects the fact that the healing microcapsules contain 2.5% epoxy (2.5% of 48 $\mu\text{m} \approx 1.20 \mu\text{m}$). Taken together we predict a theoretical maximum crack gap of about 31 μm (for 24 h). This correlates very well with the dramatic increase in healing efficiency once the crack gap is below 30 μm . For larger crack gaps, the crack faces are only partially in contact and therefore the healing efficiency is much lower.

The highest healing efficiency (and smallest crack gap) was achieved for activation schedule (c). As a rule, the longer the activation time the higher was the obtained healing efficiency and the smaller the measured crack gap after activation. However, roughly comparable results were obtained for schedules (b) and (c) save for a single test sample.

4. Conclusion

We have shown that improved healing performance can be obtained in solvent-based self-healing epoxy by using SMA wires to reduce crack face separation and provide internal heating to accelerate the healing kinetics. Healing in solvent-based systems relies on two main mechanisms: (1) matrix swelling which allows intimate contact between the separated crack faces and (2) reaction of residual functionalities which are enabled due to the presence of the released solvent. For Epon 828/DETA healed with EPA solvent the maximum crack face separation that can be healed based on solvent swelling analysis and released epoxy monomer is approximately 31 μm (after 24 h), and correlates well with experimental observation. The use of embedded SMA wires to close the crack is crucial to achieving high healing efficiency. Recovery of nearly 80% of the virgin fracture toughness was demonstrated for long-grooved TDCB specimens containing 15 wt% of microcapsules of 97.5% EPA/2.5% Epon 828.

Acknowledgments

The authors gratefully acknowledge the financial support of the Swiss National Science Foundation (FNRS 511482), the Powder Technology Laboratory (LTP) at EPFL for using their TGA and FTIR device and D. Leyvraz for his technical assistance.

References

- [1] White SR, Sottos NR, Geubelle PH, Moore JS, Kessler MR, Sriram SR, et al. Autonomic healing of polymer composites. *Nature* 2001;409(6822):794–7.
- [2] Chen X, Dam MA, Ono K, Mal A, Shen H, Nutt SR, et al. A thermally re-mendable cross-linked polymeric material. *Science* 2002;295(5560):1698–702.
- [3] Blaiszik B, Kramer S, Olugebefola S, Moore J, Sottos N, White S. Self-healing polymers and composites. *Annual Review of Materials Research* 2010;40(1):179–211.
- [4] Yuan YC, Yin T, Rong MZ, Zhang MQ. Self healing in polymers and polymer composites. Concepts, realization and outlook: a review. *Express Polymer Letters* 2008;2(4):238–50.
- [5] Bergman SD, Wudl F. Mendable polymers. *Journal of Materials Chemistry* 2008;18(1):41–62.
- [6] Trask RS, Bond IP. Biomimetic self-healing of advanced composite structures using hollow glass fibres. *Smart Materials and Structures* 2006;15(3):704–10.
- [7] Trask RS, Williams GJ, Bond IP. Bioinspired self-healing of advanced composite structures using hollow glass fibres. *Journal of the Royal Society Interface* 2007;4(13):363–71.
- [8] Toohey KS, Sottos NR, Lewis JA, Moore JS, White SR. Self-healing materials with microvascular networks. *Nature Materials* 2007;6(8):581–5.
- [9] Toohey KS, Hansen CJ, Lewis JA, White SR, Sottos NR. Delivery of two-part self-healing chemistry via microvascular networks. *Advanced Functional Materials* 2009;19(9):1399–405.
- [10] Williams HR, Trask RS, Bond IP. Self-healing composite sandwich structures. *Smart Materials and Structures* 2007;16(4):1198–207.
- [11] Williams HR, Trask RS, Bond IP. Self-healing sandwich panels: restoration of compressive strength after impact. *Composites Science and Technology* 2008;68(15–16):3171–7.
- [12] Williams GJ, Bond IP, Trask RS. Compression after impact assessment of self-healing CFRP. *Composites Part A: Applied Science and Manufacturing* 2009;40(9):1399–406.
- [13] Hansen CJ, Wu W, Toohey KS, Sottos NR, White SR, Lewis JA. Self-healing materials with interpenetrating microvascular networks. *Advanced Materials* 2009;21(41):4143–7.
- [14] Kirkby EL, Michaud VJ, Manson JAE, Sottos NR, White SR. Performance of self-healing epoxy with microencapsulated healing agent and shape memory alloy wires. *Polymer* 2009;50(23):5533–8.
- [15] Kirkby EL, Rule JD, Michaud VJ, Sottos NR, White SR, Manson JAE. Embedded shape-memory alloy wires for improved performance of self-healing polymers. *Advanced Functional Materials* 2008;18(15):2253–60.
- [16] Hayes SA, Jones FR, Marshiya K, Zhang W. A self-healing thermosetting composite material. *Composites Part A: Applied Science and Manufacturing* 2007;38(4):1116–20.
- [17] Mookhoek, SD. Novel routes to liquid-based self-healing polymer systems. Ph.D. thesis; 2010.
- [18] Caruso MM, Delafuente DA, Ho V, Sottos NR, Moore JS, White SR. Solvent-promoted self-healing epoxy materials. *Macromolecules* 2007;40(25):8830–2.
- [19] Caruso MM, Blaiszik BJ, White SR, Sottos NR, Moore JS. Full recovery of fracture toughness using a nontoxic solvent-based self-healing system. *Advanced Functional Materials* 2008;18(13):1898–904.
- [20] Blaiszik BJ, Caruso MM, McIlroy DA, Moore JS, White SR, Sottos NR. Microcapsules filled with reactive solutions for self-healing materials. *Polymer* 2009;50(4):990–7.
- [21] Brown EN, Kessler MR, Sottos NR, White SR. In situ poly(urea-formaldehyde) microencapsulation of dicyclopentadiene. *Journal of Microencapsulation* 2003;20(6):719–30.
- [22] Rule JD, Sottos NR, White SR. Effect of microcapsule size on the performance of self-healing polymers. *Polymer* 2007;48(12):3520–9.
- [23] Brown EN, Sottos NR, White SR. Fracture testing of a self-healing polymer composite. *Experimental Mechanics* 2002;42(4):372–9.
- [24] Halley PJ, Mackay ME. Chemorheology of thermosets – an overview. *Polymer Engineering & Science* 1996;36(5):593–609.
- [25] Weisenberger LA, Koenig JL. Nmr imaging of diffusion processes in polymers: measurement of the spatial dependence of solvent mobility in partially swollen PMMA rods. *Macromolecules* 1990;23(9):2445–53.
- [26] Dutheillet Y, Mantle M, Vesely D, Gladden L. Diffusion of water-acetic acid mixtures in epoxy. *Journal of Polymer Science Part B: Polymer Physics* 1999;37(23):3328–36.
- [27] Zhu M, Vesely D. The effect of polymer swelling and resistance to flow on solvent diffusion and permeability. *European Polymer Journal* 2007;43(10):4503–15.
- [28] Vesely D. Diffusion of liquids in polymers. *International Materials Reviews* 2008;53(5):299–315.